RMIT
UNIVERSITY

**Thank you for downloading this document from the RMIT Research Repository.**

The RMIT Research Repository is an open access database showcasing the research outputs of RMIT University researchers.

RMIT Research Repository: http://researchbank.rmit.edu.au/

**See this record in the RMIT Research Repository at:**

https://researchbank.rmit.edu.au/view/rmit:3937

**Version:** Published Version

**Link to Published Version:**

http://dx.doi.org/10.1260/1757-482X.1.3.217

**PLEASE DO NOT REMOVE THIS PAGE**

# Numerical Study of Particle Interaction in Gas-Particle and Liquid-Particle Flows: Part I Analysis and Validation

**K. Mohanarangam and J. Y. Tu**
School of Aerospace, Mechanical and Manufacturing Engineering
RMIT University, Vic. 3083, Australia
e-mail : Jiyuan.Tu@rmit.edu.au

## ABSTRACT

A detailed study into the turbulent behaviour of dilute particulate flow under the influence of two carrier phases namely gas and liquid has been carried out behind a sudden expansion geometry. The major endeavour of the study is to ascertain the response of the particles within the carrier (gas or liquid) phase. The main aim prompting the current study is the density difference between the carrier and the dispersed phases. While the ratio is quite high in terms of the dispersed phase for the gas-particle flows, the ratio is far more less in terms of the liquid-particle flows. Numerical simulations were carried out for both these classes of flows using an Eulerian two-fluid model with RNG based k-$\varepsilon$ model as the turbulent closure. An additional kinetic energy equation to better represent the combined fluid-particle behaviour is also employed in the current set of simulations. In the first part of this two part series, experimental results of Fessler and Eaton (1995) for Gas-Particle (GP) flow and that of Founti and Klipfel (1998) for Liquid-Particle (LP) flow have been compared and analysed. This forms the basis of the current study which aims to look at the particulate behaviour under the influence of two carrier phases. Further numerical simulations were carried out to test whether the current numerical formulation can used to simulate these varied type of flows and the same were validated against the experimental data of both GP as well LP flow. Qualitative results have been obtained for both these classes of flows with their respective experimental data both at the mean as well as at the turbulence level for carrier as well as the dispersed phases.

**Keywords:** Dilute particle flows, Gas-particle flow, Liquid-particle flow, Backward-facing step, Eulerian two-fluid model.

## INTRODUCTION:

Dilute particulate flows are encountered in a variety of industrial and natural processes irrespective of their carrier phase being gas or liquid. Particles constantly interact with the gas in industries through sand blasting equipments, pneumatic transport equipments, and also play a major role in the safe operation of the power plants, gas turbine engines and helicopters. In chemical industries they appear as reactants and catalysts, thereby controlling the order and the fate of the chemical reaction. There are even found in nature as dust dispersed in the room and as pollen released from the plants carried away by the wind. Lately there has been continued interest in these classes of flows in Bio-medical applications, to study the dust deposition patterns in realistic human nasal airway Inthavong et al.(2006) and also to aid better delivery of the medications into the human nose.

Flows with particles amid liquid are an important class of two-phase flows classified as slurry flows, whose flow systems are representative of many mineral processing operations and also provide useful operation correlations for such processes. They form an important class of flows encompassing pneumatic conveying system, turbines and machineries operating in particulate-

laden environments. These flows provide a useful tool in the simulation of sprays in industrial and natural processes, since they have comparable phase-density ratios. Comparable densities are of particular interest, since all the effects of interphase momentum transfer are important (Parthasarathy & Faeth; 1987). They also serve as a good test of methods to predict particle motion in turbulent enviroments (Parthasarathy & Faeth; 1987) as they exhibit high relative turbulence intensities for particle motion, which influence particle drag properties (Clift et al.; 1978).

Turbulence Modulation (TM) which re-defines the carrier phase both at the the velocity and at the turbulence level in the presence of dispersed phase is crucial in the design of engineering applications. However, this study is paralysed owing to the complexities of the flows and limitations of the instruments. A nearly homogenous flow like liquid-particle flow can circumvent this problem, wherein all turbulence properties are attributed due to the relative motion of the particles; thereby any change felt due to the dispersed phase on the carrier phase is a direct result of only the TM phenomenon (Parthasarthy and Faeth; 1990). This phenomenon have been exploited by many experimental researchers (Parthasarathy & Faeth; 1987, Parthasarthy and Faeth; 1990, Alajbejovic et al.; 1994, Rashidi et al.; 1990, Sato & Hishida; 1996, Ishima et al.; 2007, Borowsky & Wei; 2007, Righetti & Romano; 2007) to not only investigate, study and understand the basic features of TM but also to aid in the better formulation of numerical models. A number of previous studies have examined particle response for gas-particle flows in a sudden expansion flow experimentally (Ruck & Makiola; 1988, Hishida & Maeda; 1999, Fessler & Eaton, 1997). Whereas for the liquid-particle flows, although there have been studies in channel flow geometries, but their publication is limited for a sudden expansion geometry except for Founti & Klipfel (1998).

With the increase in the computational power and efficiency, computational fluid dynamics (CFD) have taken a centre point in offering effective solutions to not only single phase flows, but also for the simulation of wide range of two-phase flows viz., gas-particle, liquid-particle and liquid-gas flows. They not only offer a cheap solution, but also help scientists and engineers probe into places prohibitive by experimental methods or hostile environments unsuitable for human life forms. Numerical simulation of two-phase flows lie broadly into two major categories namely the Eulerian-Eulerain two-fluid model approach and the Eulerian-Lagrangian approach. In the Lagrangian approach, each particle is tracked within the computational domain, while easing the constraint of exchange co-efficients. In the Eulerain-Eulerain approach the carrier and the dispersed phases are treated as two interpenetrating continua conjoined together by exchange co-efficients.

In the Lagrangian particle tracking approach, each and every particle is tracked, thereby providing a detailed behaviour of their trajectories, velocities, bounce back angles and other parameters. Although they encompass a great deal of information with the domain, they prove to be rather cumbersome for multi-dimensional problems for the same reason being not able to track rather large number of particles given the computational power such as to obtain a good statistical information of the dispersed phase. Besides this, there is the problem of representing turbulent interactions between two phases (two-way coupling), which necessitates the need to fully understand the interactions of particles with individual vortices (Fessler & Eaton; 1997).

Eulerian-Eulerian approach constituted by Anderson and Jackson (1967), Ishii (1975), regard the carrier and the dispersed phases as two interacting fluids with momentum and energy exchange between them. One major advantage of using the Eulerian approach is that the well-proven numerical procedures for single-phase flows can be directly extended to the secondary phase with the effects of turbulent interactions between the two fluids, lately there are considerations of extending the Eulerian two-fluid model by adopting the large eddy simulation (LES) approach (Pandya & Mashayek; 2002). Shirolkar et al (1996) in their paper stated that Eulerian models have problems to account for the particle history effects as they do not re-trace the motion of individual particles together. They also suffer from continuum assumption problems with respect to particles, as the particles equilibrate with neither local fluid nor each other when flowing through the flow field. In addition, crossing trajectories become more pronounced as particle inertia increases and Eulerian methods may become less accurate with increasing Stokes number, so a priori and rudimentary Lagrangian calculations should always be performed to check its validity. To overcome the problem of modeling particle–wall collision, Tu and Fletcher (1995) established a set of Eulerian formulation with generalized wall boundary conditions and developed a particle–wall collision model to better represent the particle–wall momentum transfer, wherein a good agreement with the experimental data was achieved. Using this model, further investigation into the particle-

laden flow in an in-line tube bank (Tu et al,; 1998) was carried out, which also resulted in good agreement with the experimental data. It was generally noticed that Eulerian two fluid modelling is more suitable for engineering applications, whereas the Eulerian–Lagrangian approach is a good research tool for examining fundamental processes and verifying closure laws derived for the Eulerian–Eulerian approach (Pawel et al.; 2005).

Numerical simulation of gas-particle/liquid-particle flows have been performed by various researchers, as separate entities using both the Lagrangian tracking and the Eulerian two-fluid models. There are a diverse range of techniques formulated and applied to simulate the same in the literatures. In our current study, we would confide ourselves to only the numerical work carried out, with respect to the two sets of experimental data (Fessler & Eaton; 1999, Founti & Klipfel; 1998) used to validate our simulations. Fessler and Eaton's (1999) experimental data was simulated using an improved stochastic separated flow (ISSF) model (Chan et al.; 2001) and was compared with two other widely used trajectory models namely, the Determistic Separated Flow (DSF) and the Stochastic Separated Flow (SSF) model (Zhang et al.; 2002). Both of the above mentioned simulations were performed using a RANS (Reynolds Averaged Navier-Stokes) approach, while LES simulation was also performed (Yu et al.; 2004) to validate the same set of experimental data later. An extensive Eulerian two-fluid model simulation (Mohanarangam & Tu; 2007) was performed by the current authors and the same was validated not only against the velocities and the turbulence of the two phases, but also was the TM simulated and studied against the experimental data of Fessler and Eaton (1997). Numerical simulations to validate the experimental data of Klipel and Founti (1998) was  done by the same authors using the Lagrangian tracking approach, however they have been serious under and over-predictions caused by the numerical simulations, which makes one  conclude that still there remain problems that hamper the prediction of particle response.  Similar numerical approach (Chen & Pereira; 2001) have been adopted to simulate the flow but using an eddy-interaction model developed by Gosman and Ioannides (Gosman & Ionnides; 1981), while the mean particle velocities showed good comparison, they have been still problems in predicting the particulate turbulence qualitatively; this is majorly attributed to the eddy interaction models generally used to simulate dispersed phase flows using the Lagrangian tracking approach.

In the first part of this series, two varying sets of experimental data behind a backward facing step geometry have been analysed. The main difference between them is the fact that the density of the carrier phases between the two sets is quite different with a comparable density ratio of almost 1:700.  It is quite low for the GP flows and higher in case of LP flows. The main idea is to investigate whether the particles of the same density behave in a similar pattern under the influence of two carrier phases. Experimental comparison and investigation is carried out both at the mean velocity as well as at the turbulence level. This section which outlines the particulate response amidst two carrier phases serves as the main reason to undertake this study as the ratio between the carrier and dispersed phases is about 1:2137 for GP flows, while for the LP they are in the ratio of 1:3. The numerical model is outlined first, followed by the numerical procedure adopted for simulating two different sets of experimental data (Fessler and Eaton; 1995, Founti and Klipfel; 1998). The code verification section verifies whether the code would be able to replicate the two variants of experimental data used in the current study.

## NUMERICAL MODEL:

The modified Eulerian two-fluid model developed by Tu & Fletcher (1995) and Tu (1997) used in this study considers the fluid and particle phases as two interpenetrating continua. Hereby, a two way coupling is achieved between the dispersed and the carrier phases.

The underlying assumptions employed in the current study are:
1)     The particulate phase is dilute and consists of mono disperse spherical particles.
2)     For such a dilute flow, the fluid volume fraction is approximated by unity.
3)     The viscous stress and the pressure of the particulate phase are negligible.
4)     The flow field is isothermal.

In the Eulerian model both the carrier and the dispersed phases are treated as a continuum, with the necessity to solve a set of Reynolds-averaged conservation equations for mass, momentum, turbulent kinetic energy as well as its dissipation. The generic transport form of these equations for property $\phi$  in the three dimensional form can be written as

$$\frac{\partial \phi}{\partial t} + \frac{\partial (u\phi)}{\partial x} + \frac{\partial (v\phi)}{\partial y} + \frac{\partial (w\phi)}{\partial z} = \frac{\partial}{\partial x}\left[ _{\phi}\frac{\partial \phi}{\partial x}\right] + \frac{\partial}{\partial y}\left[ _{\phi}\frac{\partial \phi}{\partial y}\right] + \frac{\partial}{\partial z}\left[ _{\phi}\frac{\partial \phi}{\partial z}\right] + S_{\phi} \qquad (1)$$

Equation 1 represents the various physical transport processes occurring in the fluid flow, with the local acceleration and advection terms on the left hand side being equal to the diffusion term ($\Gamma$ = diffusion coefficient) and source term ($S_{\phi}$) on the right hand side. By varying the values of $\phi$, $\Gamma_{\phi}$, $S_{\phi}$ the relevant continuity, momentum, turbulence energy and dissipation equations can be obtained.

**Fluid Phase Modelling:**
Table 1 show these values for the gas phase, in addition to the normal source terms obtained from the single phase, additional terms arise as a result of the dispersed phase so as to render an effective two-way coupling.

Table 1: Fluid phase equations

| $\phi$ | $\Gamma_{\phi}$ | $S_{\Phi}$ |
|--------|-----------------|------------|
| 1 | 0 | 0 |
| $u_f$ | $v_f + v_{fT}$ | $-\frac{1}{\rho_f}\frac{\partial p_f}{\partial x} - F_D^u$ |
| $v_f$ | $v_f + v_{fT}$ | $-\frac{1}{\rho_f}\frac{\partial p_f}{\partial y} - F_D^v$ |
| $w_f$ | $v_f + v_{fT}$ | $-\frac{1}{\rho_f}\frac{\partial p_f}{\partial z} - F_D^w$ |
| $k_f$ | $\dfrac{v_{fT}}{\sigma_k}$ | $P_f - D_f - S_k$ |
| $\varepsilon_f$ | $\dfrac{v_{fT}}{\sigma_\varepsilon}$ | $\dfrac{\varepsilon}{k}\left(C_{\varepsilon 1}P_f - C_{\varepsilon 2}D_f\right) - R - S_\varepsilon$ |

Here $\rho_f$, $u_f$ and $p_f$ are the bulk density, mean velocity and mean pressure of the fluid phase, respectively. $v_f$ is the laminar viscosity of the fluid phase. $F_D$ is the Favre-averaged aerodynamic drag force due to the slip velocity between the two phases and is given by

$$F_D = \rho_p \frac{f(u_f - u_p)}{t_p} \qquad (2)$$

where the correction factor 'f' is selected according to Schuh et al (1989)

$$f = \begin{cases} 1 + 0.15\,Re_p^{0.687} & 0 < Re_p \leq 200 \\ 0.914\,Re_p^{0.282} + 0.0135\,Re_p & 200 < Re_p \leq 2500 \\ 0.0167\,Re_p & 2500 < Re_p \end{cases} \qquad (3)$$

Table 2: Particulate phase equations

| $\phi$ | $\Gamma_\phi$ | $S_\phi$ |
|---|---|---|
| $\rho_p$ | $0$ | $0$ |
| $u_p$ | $\nu_{pT}$ | $F_D^u + F_G^u + F_{WM}^u$ |
| $v_p$ | $\nu_{pT}$ | $F_D^v + F_G^v + F_{WM}^v$ |
| $w_p$ | $\nu_{pT}$ | $F_D^w + F_G^w + F_{WM}^w$ |
| $k_p$ | $\dfrac{\nu_{pT}}{\sigma_k}$ | $P_p - I_{fp}$ |
| $k_{fp}$ | $\dfrac{\nu_{pT}}{\mathrm{Pr}_T}$ | $P_{fp} - \overline{\rho}_p \varepsilon_{fp} - II_{fp}$ |
| $\varepsilon_{fp}$ | $\dfrac{\nu_{pT}}{\sigma_\varepsilon}$ | $\dfrac{\varepsilon_f}{k_f}\left(C_{\varepsilon 1}P_{fp} - C_{\varepsilon 2}D_{fp}\right)$ |

with the particle response or relaxation time given by $t_p = \rho_s d_p^2/18\rho_f \nu_{fl})$ where $\rho_s$ is the particle material density and the particle Reynolds number given by $\mathrm{Re}_p = \dfrac{\rho_p d_p |u_p - u_f|}{\mu_f}$ wherein $d_p$ is the diameter of the particle.

For the carrier fluid phase, which uses an eddy-viscosity model, $\nu_{fT}$ the turbulent or 'eddy' viscosity of the fluid phase is computed from $\nu_{fT} = C_\mu(k_f^2/\varepsilon_f)$ . The kinetic energy of the turbulence, $k_f$ and its dissipation rate, $\varepsilon_f$ are governed and solved by separate transport equations. The RNG version of $k$-$\varepsilon$ model is employed in the current study and by which the rate of strain term R in the $\varepsilon_f$ equation is expressed as

$$R = \frac{C_\mu \eta^3(1 - \eta/\eta_o)}{1 + \beta\eta^3}\frac{\varepsilon_f^2}{k_f}, \quad \eta = \frac{k_f}{\varepsilon_f}(2S_{ij}^2)^{1/2}, S_{ij} = \frac{1}{2}\left(\frac{\partial u_f^i}{\partial x_j} + \frac{\partial u_f^j}{\partial x_i}\right) \quad (4)$$

where $\beta = 0.015$, $\eta_o = 4.38$. The major endeavour of including this term is to take into account the effects of rapid strain rate along with the streamline curvature, which in many cases the standard $k$-$\varepsilon$ turbulence model fails to predict. The constants in the turbulent transport equations are given by $\alpha = 1.3929$, $C_\mu = 0.0845$, $C_{\varepsilon 1} = 1.42$ and $C_{\varepsilon 2} = 1.68$ as per the RNG theory (1983).

For the confined two-phase flow, the effects of the particulate phase on the turbulence of the fluid phase are taken into account through the additional terms $S_k$ and $S_\varepsilon$ in the $k_f$ and $\varepsilon_f$ equations which arise from the correlation term given by

$$S_k = (\overline{-u'_f F'_D}) = -\frac{2f}{t_p}\rho_p(k_f - k_{fp}) \quad (5)$$

in the $k_f$ equation and

$$S_\varepsilon = -2\nu_{fl}\overline{\frac{\partial u'_f}{\partial x_j}\frac{\partial F'_D}{\partial x_j}} = -\frac{2f}{t_p}\rho_p(\varepsilon_f - \varepsilon_{fp})$$

(6)

in the $\varepsilon_f$ equation, where $k_{fp}$ and $\varepsilon_{fp}$ will be presented in the next following section discussing the particulate turbulence modeling.

**Particle Phase Modelling:**

Table 2 depicts the particulate equations and also their relevant source terms used in our current study. In the particulate momentum equations there are three additional terms representing aerodynamic drag force ($F_D$), the gravity force ($F_G$) and the wall-momentum transfer force ($F_{WM}$) due to particle-wall collisions, respectively. The gravity force is given by $F_G=\rho_p g$, where g is the gravitational acceleration.

The particulate turbulent kinetic energy is similar to the gas phase except for the absence of the laminar viscosity and also with the inclusion of different set of source terms $P_p$ and $I_{fp}$. The production term $P_p$ is modelled using the formulation

$$P_p = \rho_p \nu_{pt}(\frac{\partial u_p^i}{\partial x_j} + \frac{\partial u_p^j}{\partial x_i})\frac{\partial u_p^i}{\partial x_k} - \frac{2}{3}\rho_p\delta_{ij}(k_p + \nu_{pt}\frac{\partial u_p^k}{\partial x_k})\frac{\partial u_p^i}{\partial x_k}$$

(7)

while the turbulence interaction between two phases $I_{fp}$ is given by

$$I_{fp} = \frac{2f}{t_p}\rho_p(k_p - k_{fp})$$

(8)

$k_{fp} = \frac{1}{2}\overline{u_f^i u_p^i}$ is the turbulence kinetic energy interaction between two phases. The production $P_{fp}$ term resulting from co-variance is given by

$$P_{fp} = \{\rho_p(\nu_{ft}\frac{\partial u_f^i}{\partial x_j} + \nu_{pt}\frac{\partial u_p^j}{\partial x_i}) - \frac{2}{3}\rho_p\delta_{ij}k_{fp} - \frac{1}{3}\bar{\rho}_p\delta_{ij}(\nu_{ft}\frac{\partial u_p^k}{\partial x_k} + \nu_{pt}\frac{\partial u_p^k}{\partial x_k})\}(\frac{\partial u_f^i}{\partial x_j} + \frac{\partial u_p^i}{\partial x_j})$$

(9)

while the turbulence interaction between two phases $I_{fp}$ is given by

$$II_{fp} = \frac{f}{2t_p}\rho_p[(1+m)2k_{fp} - 2k_f - m2k_p]$$

The turbulent eddy viscosity of the particulate phase, $\nu_{pT}$, is defined in a similar way as the gas phase as:

$$\nu_{pT} = \frac{2}{3}k_p t_{pt} = l_{pt}\sqrt{\frac{2}{3}k_p}$$

(10)

The turbulent characteristic length of the particulate phase is modeled by $l_{pt} = \min(l'_{pt}, D_s)$ where $l'_{pt}$ is given by

$$l'_{pt} = \frac{l_{ft}}{2}(1 + \cos^2 \theta)\exp[-B_{fp}\frac{|u'_r|}{|u'_g|}sign(k_f - k_p)]$$  (11)

where $\theta$ is the angle between the velocity of the particle and the velocity of the gas to account for the crossing trajectories effect (Huang et al.;1993) $B_{fp}$ is an experimentally determined constant, which takes a value of 0.01. $D_s$ is the characteristic length of the system and provides a limit to the characteristic length of the particulate phase.

The relative fluctuating velocity is given by

$$u'_r = u'_f - u'_p$$  (12)

and

$$|u'_r| = \sqrt{\overline{u'^2_f} - 2\overline{u'_f u'_p} + \overline{u'^2_p}} = \sqrt{\frac{2}{3}(k_f - 2k_{fp} + k_p)}$$  (13)

## NUMERICAL PROCEDURE

All the transport equations are discretized using a finite volume formulation in a generalized coordinate space, with metric information expressed in terms of area vectors. The equations are solved on a non-staggered grid system, wherein all primitive variables are stored at the centroids of the mass control volumes. Third-order QUICK scheme is used to approximate the convective terms, while second-order accurate central difference scheme is adopted for the diffusion terms. The velocity correction is realized to satisfy continuity through SIMPLE algorithm, which couples velocity and pressure. At the inlet boundary the particulate phase velocity is taken to be the same as the fluid velocity. The concentration of the particulate phase is set to be uniform at the inlet. At the outlet the zero streamwise gradients are used for all variables. The wall boundary conditions are based on the model of Tu & Fletcher (1995).

All the governing equations for both the carrier and dispersed phases are solved sequentially at each iteration, the solution process is started by solving the momentum equations for the fluid phase followed by the pressure-correction through the continuity equation, turbulence equations for the fluid phase, are solved in succession. While the solution process for the particle phase starts by the solution of momentum equations followed by the concentration then fluid-particle turbulence interaction to reflect the two-way coupling, the process ends by the solution of turbulence equation for the particulate phase. At each global iteration, each equation is iterated, typically 3 to 5 times, using a strongly implicit procedure (SIP). The above solution process is marched towards a steady state and is repeated until a converged solution is obtained.

## RESULTS AND DISCUSSION
### Analysis of experimental data:

In this section, the experimental data at the mean and turbulence level are analysed in order to understand the particle behaviour in relation to its carrier phase namely the gas and the liquid. For this purpose, five sections were selected, aft of the sudden expansion, one near the step (section before the re-attachment point) another almost at the middle (a section aft of the re-attachment point) and the other farther away from the step nearing the exit of the geometry. Figure 1a shows the backward facing step geometry, which is similar to the one used in the experiments of Fessler and Eaton (1995), comprising of a step height (h) of 26.7mm. As the span wise z-direction perpendicular to the paper is much larger than the y-direction used in the experiments, the flow is considered to be essentially two-dimensional. The backward facing step has an expansion ratio of 5:3. The Reynolds number over the step works out to be 18,400 calculated based on the centerline velocity and step height (h). The experimental set up of Founti and Klipfel (1998) consisted of a pipe flow with a sudden expansion ratio of 1:2, with a step height of 25.5mm, as depicted in figure 1b, working at a Reynolds number of 28,000. The summary of the flow conditions along with the properties of the dispersed phase particles used in this study are summarized in Table 3.
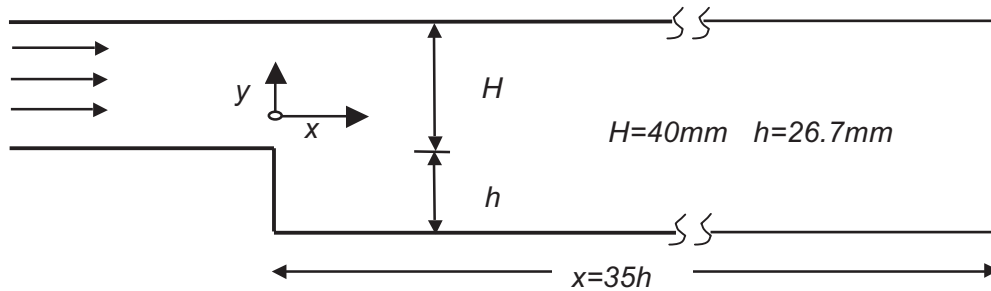
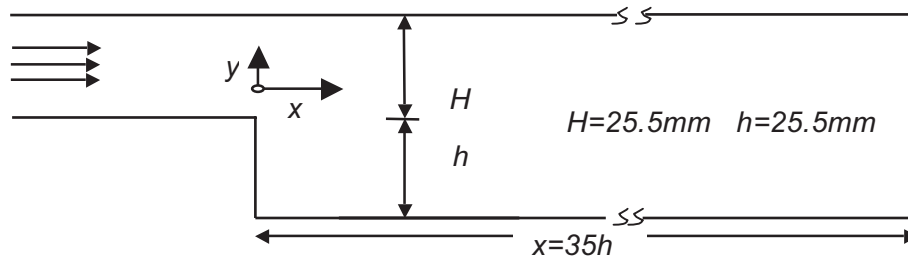Figure 1a. Backward facing step geometry (Fessler & Eation; 1997)



Figure 1b. Backward facing step geometry (Founti & Klipfel; 1998)

Table 3. Flow properties of carrier and dispersed phases for LP & GP flows

| Parameters | Gas-Particle (GP) flow Fessler & Eaton | Liquid-Particle (LP) flow Founti & Klipfel |
|---|---|---|
| | | |
| Reynolds number ($Re_h$) | 18,700 | 28,000 |
| Geometry | BFS | Pipe (BFS) |
| Continuous Phase | Air | Diesel Oil |
| Mass loading | 20% | 15% |
| Particle Density | 2500 | 2500 |
| Particle Diameter | 150 micron | 450 micron |
| Phase-density ratio | 2137:1 | 3.0:1 |
| | | |

An important, dimensionless scaling parameter in defining on how the particles behave with the flow field is the Stokes number ($St$), which is given by the ratio of the particle relaxation time to a time characteristic of the fluid motion, i.e., $St = t_p/t_s$. This determines the kinetic equilibrium of the particles with the surrounding fluid. In choosing, the fluid time scale $t_s$, amidst the complexity of having two different geometries with different expansion ratios and also with the re-attachment length varying with the addition of the particles, the fluid time scales were determined by $t_s = 5h/U_o$ in lieu with the experimental conditions of Fessler and Eaton (1997). A small stokes number ($St \ll 1$) signifies that the particles are in near velocity equilibrium with the carrier fluid. For larger stokes number ($St \gg 1$) particles are no longer in equilibrium with the surrounding fluid phase, which will be exemplified in the later sections. Based on the above definition of Stokes number, the Stokes number for the GP and the LP flow examined in our study work out to be 14.2 and 0.59 respectively.

Figures 2a-e shows the mean streamwise velocities of the liquid and particle phase flows as presented from the experiments of Founti & Klipfel (1998), the plots also show the height of the step along the length of the Y-axis for a height of y/h=1.0. It can be seen at section x/h=0.7, the particles seem to exhibit a higher negative velocity for a section of y/h<1, while for a small region at the proximity of the step they seem to exhibit a homogeneous behaviour. After this height the particles seem to surpass the liquid velocities for the section y/h>1 and this feature is mainly due to the fact that particles exhibit more inertial than the carrier liquid. At section x/h=5.9, the particles seem to exhibit a positive velocity than the carrier phase below the step, whereas for the rest of the height of the geometry they tend to behave in unison. At section x/h=7.8, which is almost the middle section, the liquid phase has a higher negative velocity than that of the particulate phase, this behaviour seems to follow for a height of up to y/h=1, after which the both phases seem to behave in unison. For section x/h=11.8, it can be seen that the particles get displaced more than the liquid for section below the step, whereas for section above the step they exhibit a tandem behaviour. At the final section x/h= 15.7 the particles and the liquid seem to part more away from the bottom of the step, for which a difference is felt until a height of y/h=1.5.
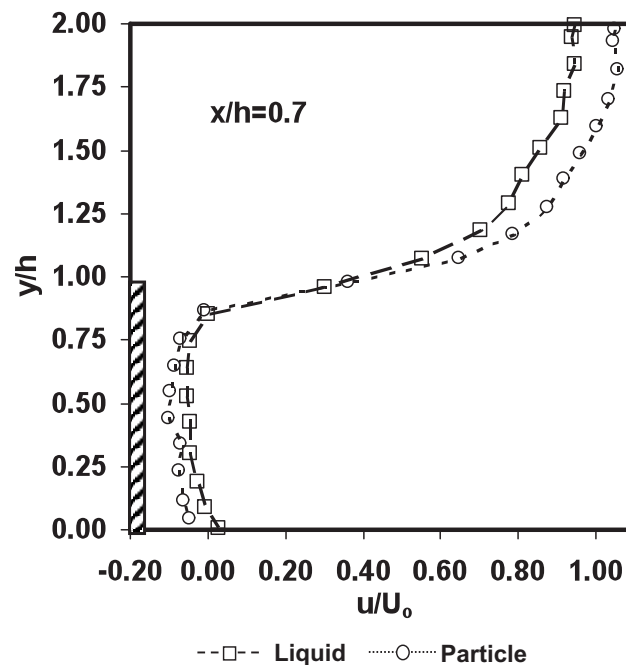


Figure 2a. Experimental mean streamwise velocities at x/h=0.7 for liquid-particle flow
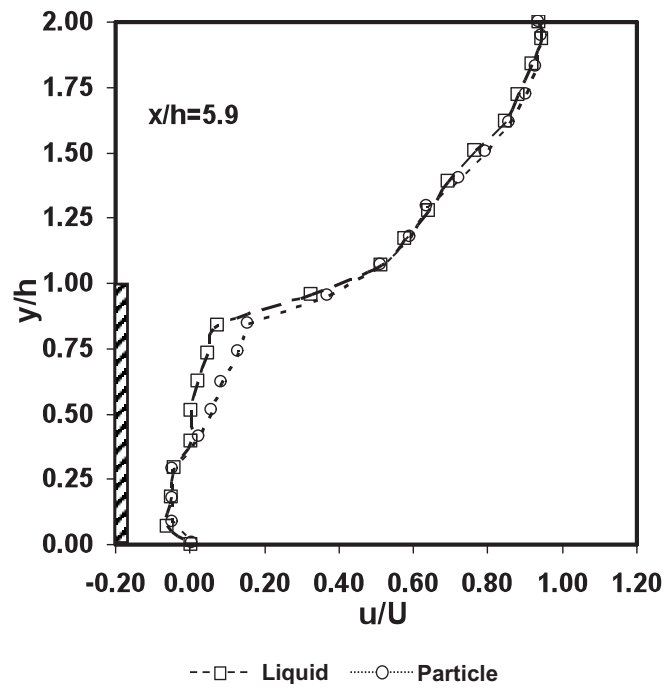
Figure 2b. Experimental mean streamwise velocities at x/h=5.9 for liquid-particle flow
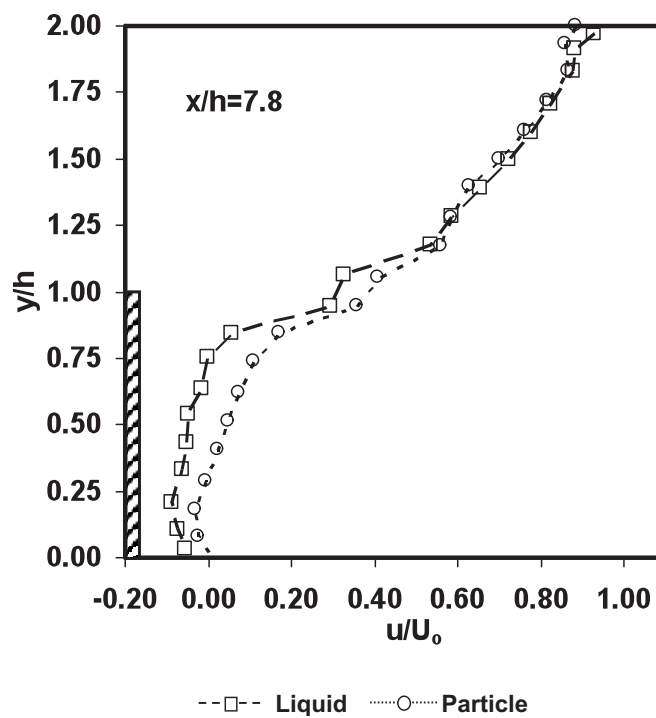


Figure 2c. Experimental mean streamwise velocities at x/h=7.8 for liquid-particle flow
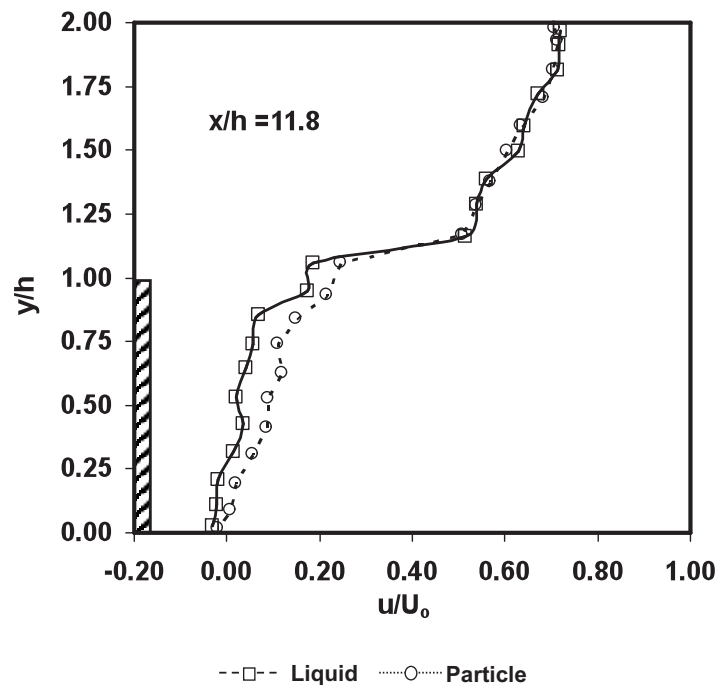
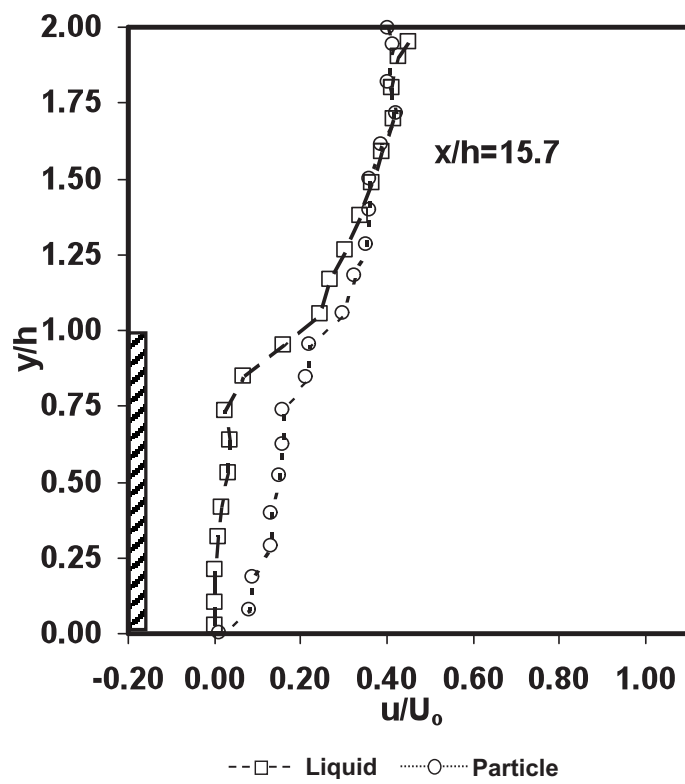Figure 2d. Experimental mean streamwise velocities at x/h=11.8 for liquid-particle flow



Figure 2e. Experimental mean streamwise velocities at x/h=15.7 for liquid-particle flow

Figures 3a-e show the mean velocities of the GP flow as obtained from the experiments of Fessler and Eaton (1995). It can be seen that the section above the step is more in this case compared to the previous experimental geometry due to the step expansion ratios being different. Figure 3a depicts the section x/h=2, just aft of the step, it can be observed that for the section below the step there exists no particles quite contrast to the previous experimental result (Founti & Klipfel; 1998). This is mainly attributed to the fact that the particles in this case have a higher Stokes number, and thereby exhibit more inertial compared to the LP flows. For sections above the step it can be seen that the particles lag behind the gas velocities. For section x/h=5 (figure 3b) fewer particles can be seen for a small section below the step, the particles here try to lead for some section above the step and later lag behind the gas. At section x/h=7, the middle section of the geometry close to the re-attachment point, the particle velocities seem to 'catch up' with that of the gas phase and their velocities are more or less the same, however this feature does not last long as at section x/h=9 the particles show a mixed behaviour in relation to the gas phase. At the exit of the backward-facing step geometry (x/h=14), where the flow recovers from the re-circulation and also the related pressure gradients, a clearly marked difference in velocities is observed, wherein the particles seem to overtake the gas due to its inertial.

From the two sets of experimental results outlined above, one could observe that at near the inlet sections, where the re-circulation is quite predominant for both the cases, particles seem to lag behind the gas for the GP flows, while exhibiting a higher inertial with respect to the LP flows, where in, the particles lead throughout the height of the step. Overall, with respect to the magnitude of the mean velocities, the particles seem to exhibit more or less a change in the pattern from 'lead' to 'lag', above the step as one proceed along the step for LP flows, whereas the particles seem to exhibit the opposite pattern from 'lag' to 'lead' for GP flows along the step.
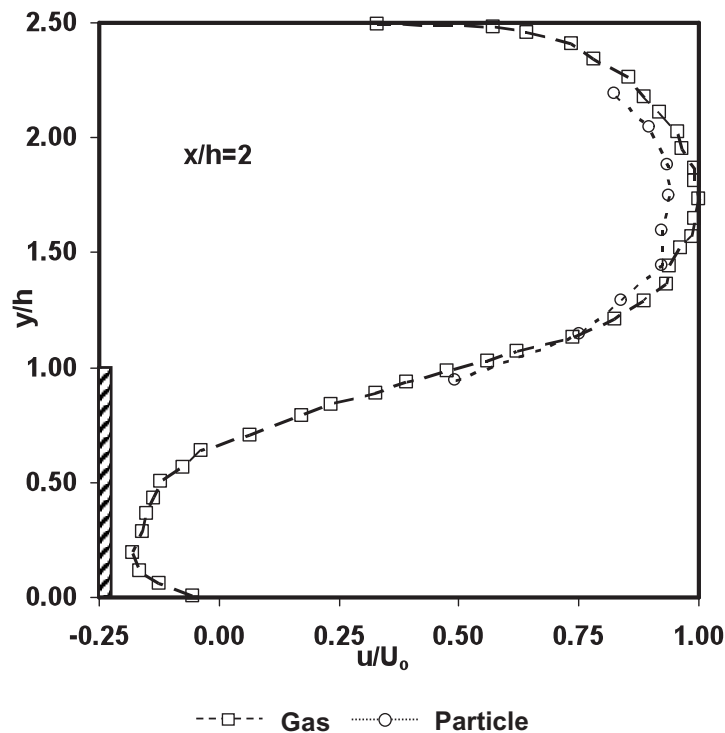


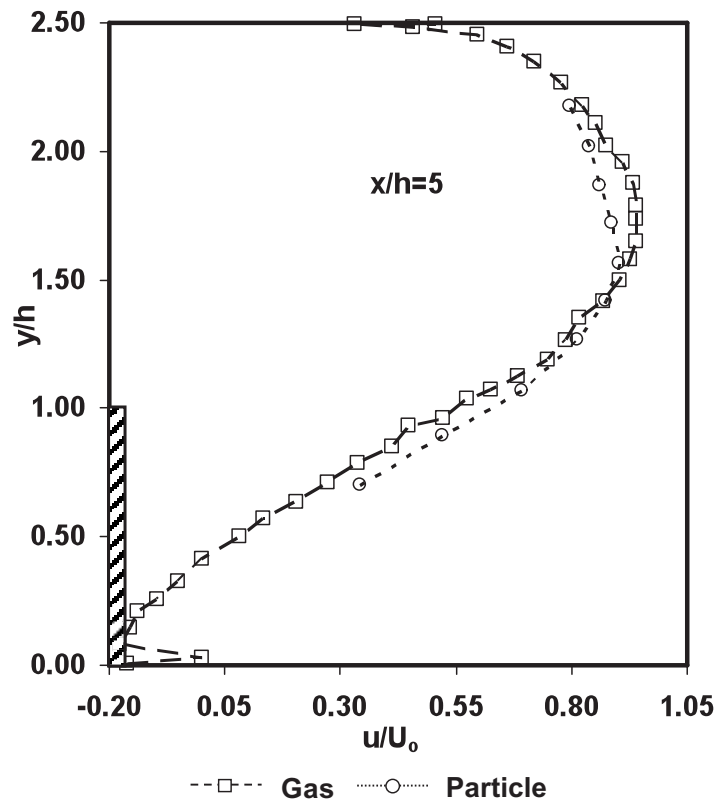Figure 3a. Experimental mean streamwise velocities at x/h=2 for gas-particle flow

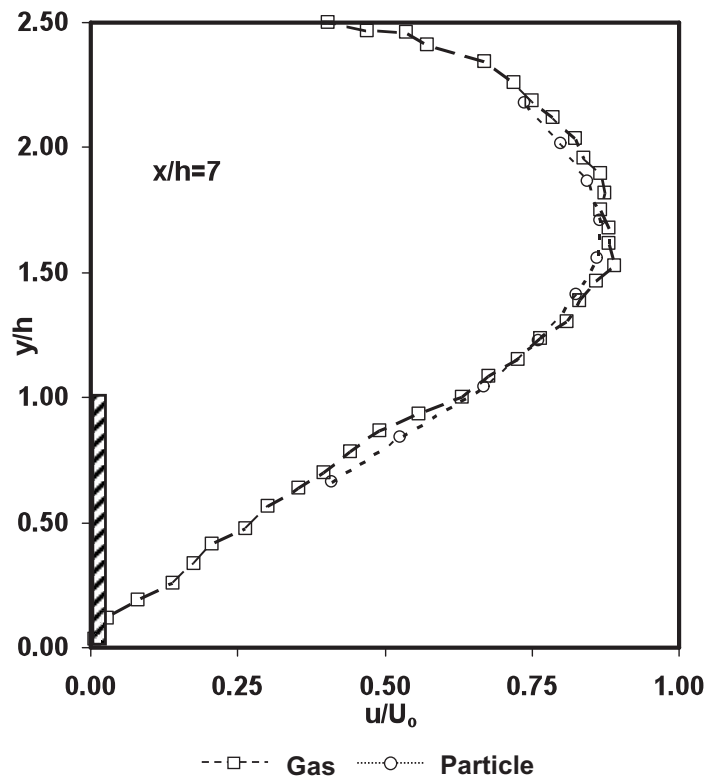Figure 3b. Experimental mean streamwise velocities at x/h=5 for gas-particle flow



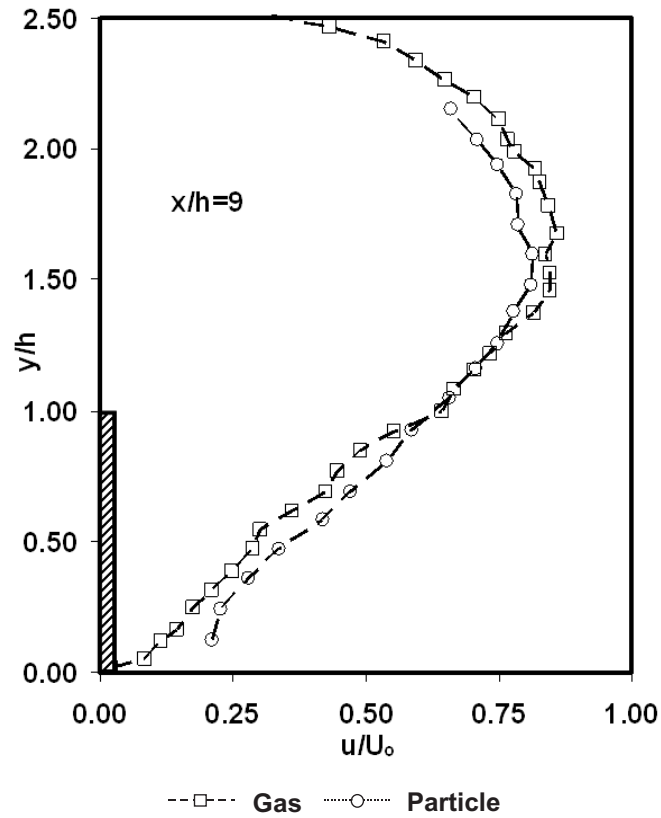Figure 3c. Experimental mean streamwise velocities at x/h=7 for gas-particle flow

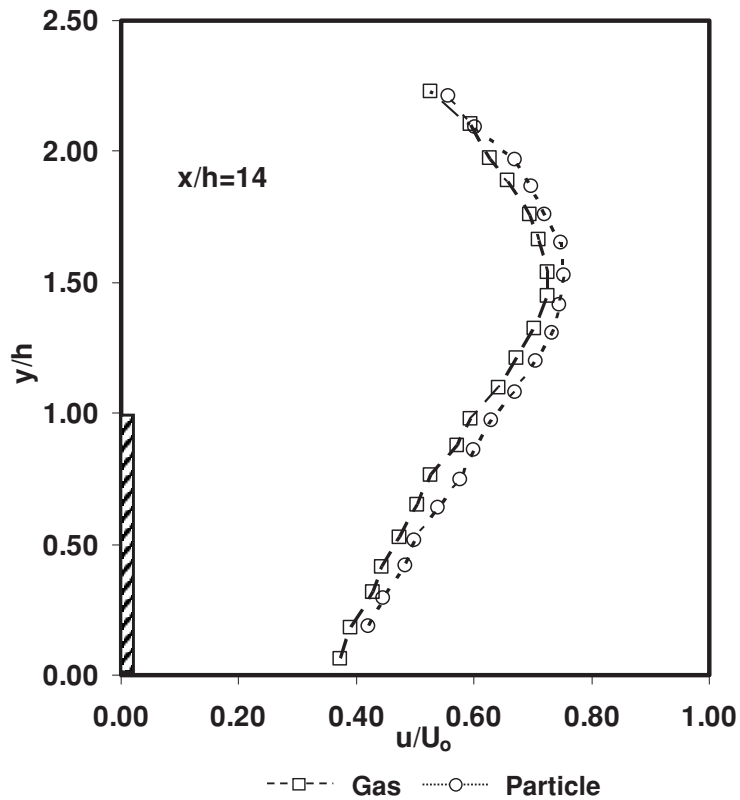Figure 3d. Experimental mean streamwise velocities at x/h=9 for gas-particle flow

Figure 3e. Experimental mean streamwise velocities at x/h=14 for gas-particle flow

In order to understand better this behaviour we now turn to the mean streamwise fluctuations for these two kinds of flows. Figures 4a-e shows the fluctuating velocities of LP flows and it can be seen that at the entry (x/h =0.7) the particles seem to 'lag' behind the liquid for a height of y/h>1, while showing an increase with respect to liquid in the lower part. A little further away at section x/h=5.9 the carrier and the dispersed phase exhibit a similar behaviour to the previous section, with the particle fluctuation taking a reverse pattern at the step height. For the middle section considered (x/h=7.8), for a height of about y/h>1 they exhibit a homogenous flow behaviour, whereas at the lower part the particles again seem to exceed its liquid counterpart. In all the three previous sections, for a step height of y/h<1 the particles show an increasing trend of moving away from liquid as one passes away from the step in the streamwise direction. At section x/h=11.8, it could be seen that the particles have come closer to the liquid for a section of y/h<1, whereas they behave in unison above the step. At the exit of the geometry, both the continuous and dispersed phases have almost the same pattern for a section of y/h<0.75, where in the particles have moved even closer to the liquid in comparison to the previous section, prompting the fact that the particle 'catch up' with the liquid phase, mimicking a homogenous flow pattern.
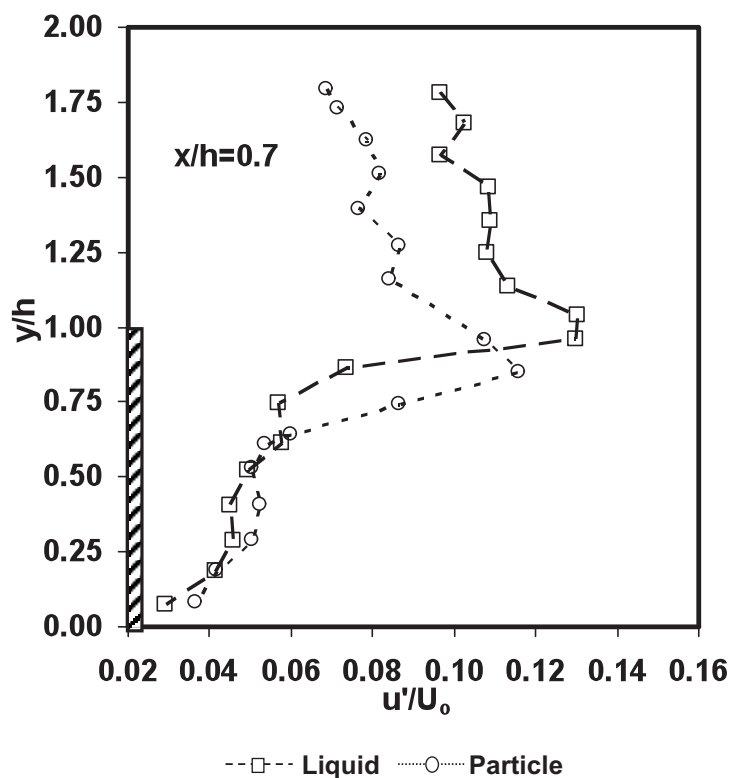


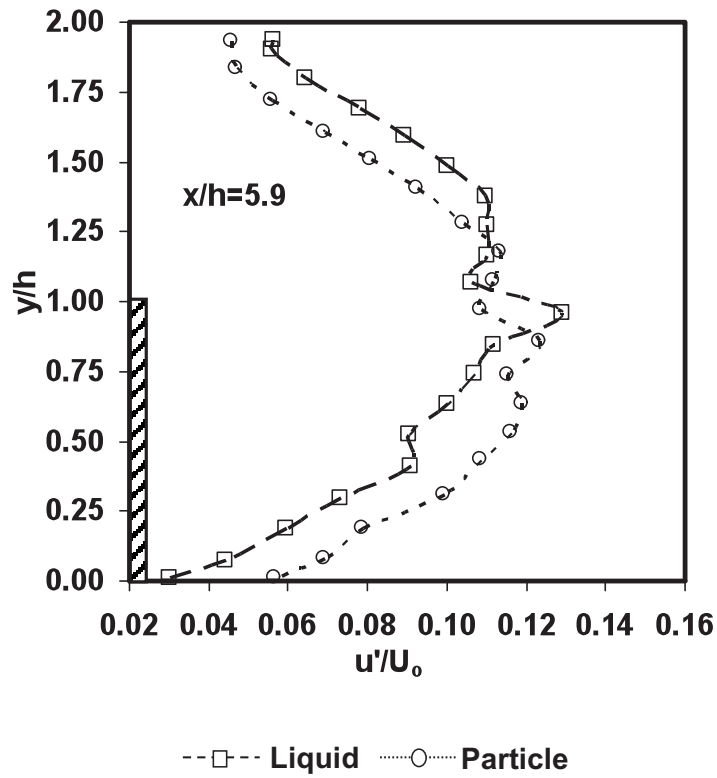Figure 4a. Experimental mean fluctuating velocities at x/h=0.7 for liquid-particle flow

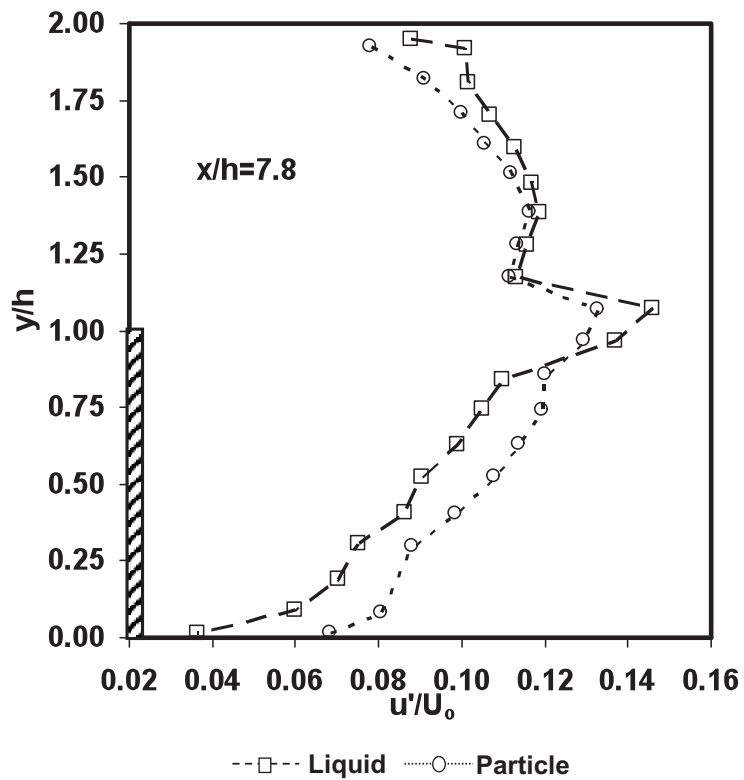Figure 4b. Experimental mean fluctuating velocities at x/h=5.9 for liquid-particle flow



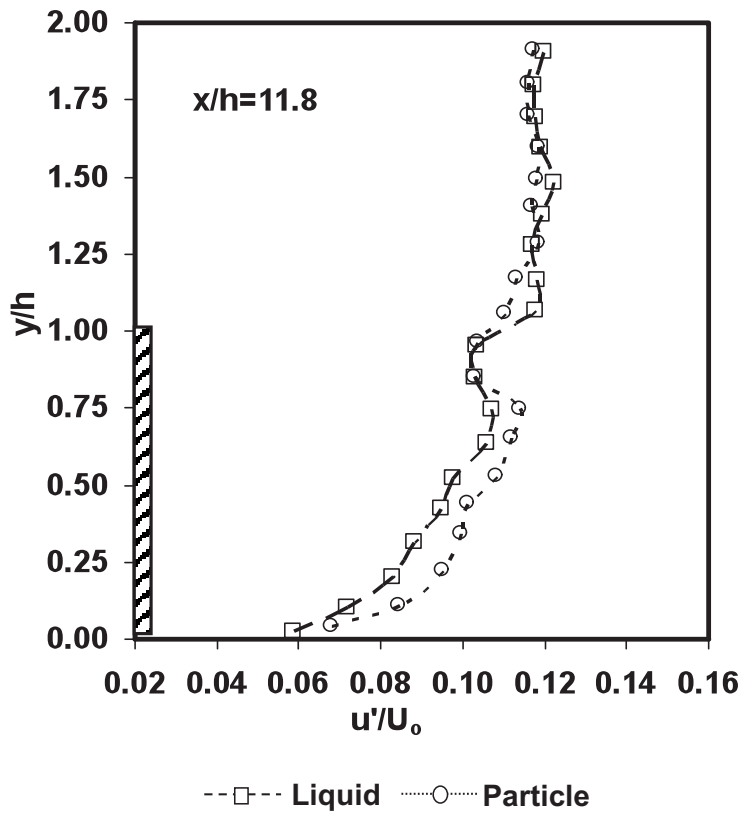Figure 4c. Experimental mean fluctuating velocities at x/h=7.8 for liquid-particle flow

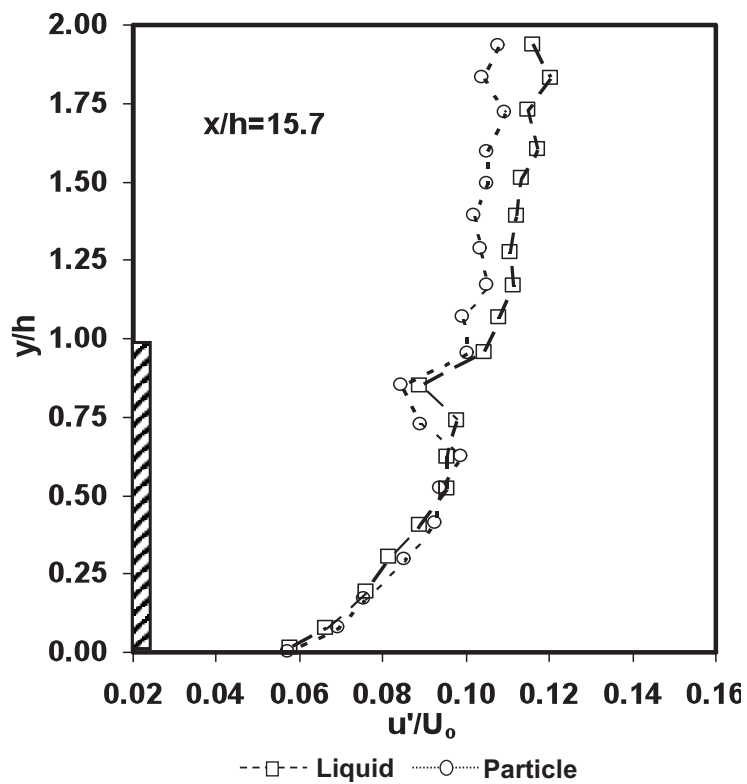Figure 4d. Experimental mean fluctuating velocities at x/h=11.8 for liquid-particle flow



Figure 4e. Experimental mean fluctuating velocities at x/h=15.7 for liquid-particle flow

Figures 5a-e show the fluctuation results for the GP flow, at the entry section x/h=2, it can be seen that the particulate phase has a much higher fluctuating velocity in comparison to the gas phase, with the particulate phase showing a fluctuation of almost 500% at a height of y/h=1.75. This is mainly attributed to the high inertial velocity exhibited by the particles. For a section of x/h=5.0 the particles again exhibit a higher fluctuating velocity for a step height of greater than 1.5, below which the particles and the gas behave in cohesion. However the maximum difference is about 200% again at a height of y/h=1.75. At section x/h=7 near the re-attachment point, the parity between the carrier and dispersed phase is quite subtle, as the particles move closer to the fluctuating velocities of the gas. While at section x/h=9, the fluctuating velocities of the particle phase move even closer to the carrier gas phase. As more particles could be seen below the step they exhibit a mixed behaviour for the section y/h<1. Near the exit of the geometry at section x/h=14, it is observed that both the dispersed and the continuous phase seem to fluctuate in unison, as the particles almost catch up fully with the gas phase. From the above experimental results of the fluctuation, it can be ascertained that the particle 'lag' behind with respect to the continuous phase in terms of LP flows, whereas they 'lead' in terms of the gas-particle flows.
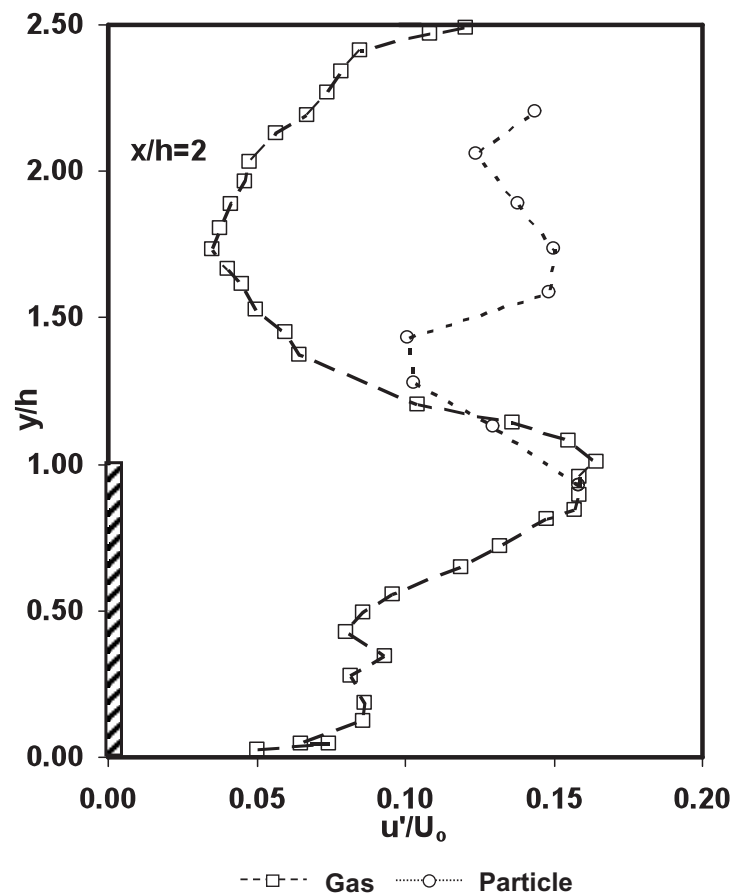


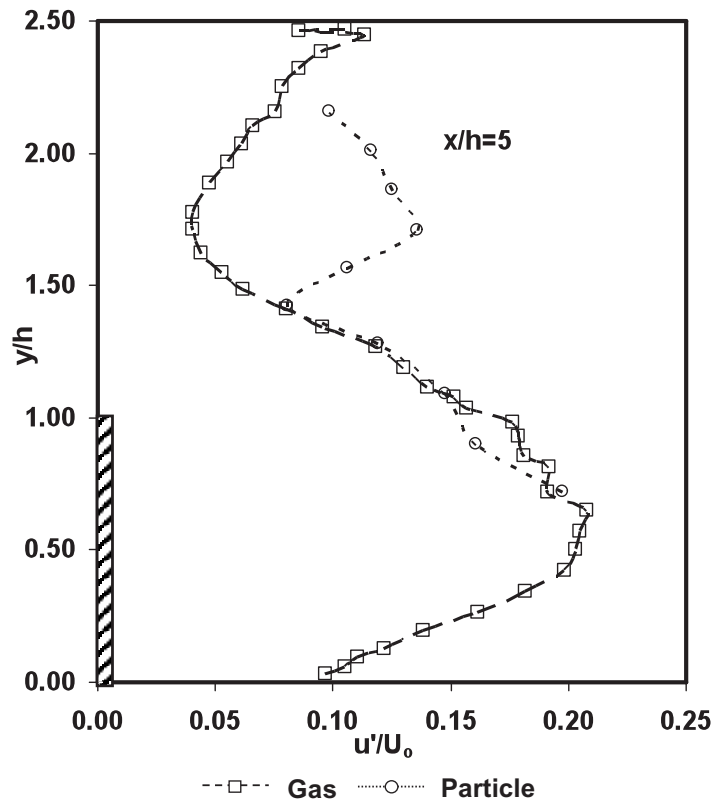Figure 5a. Experimental mean fluctuating velocities at x/h=2 for gas-particle flow

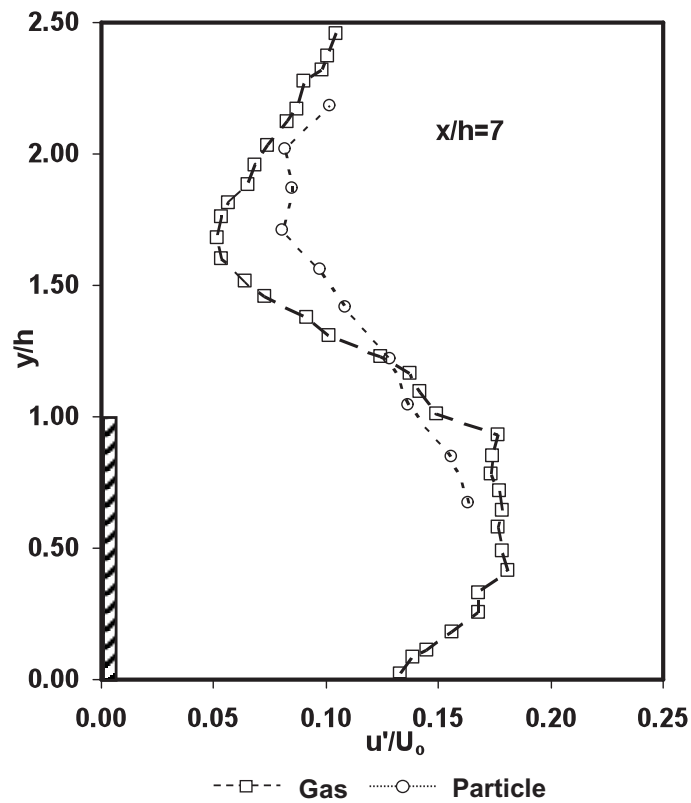Figure 5b. Experimental mean fluctuating velocities at x/h=5 for gas-particle flow



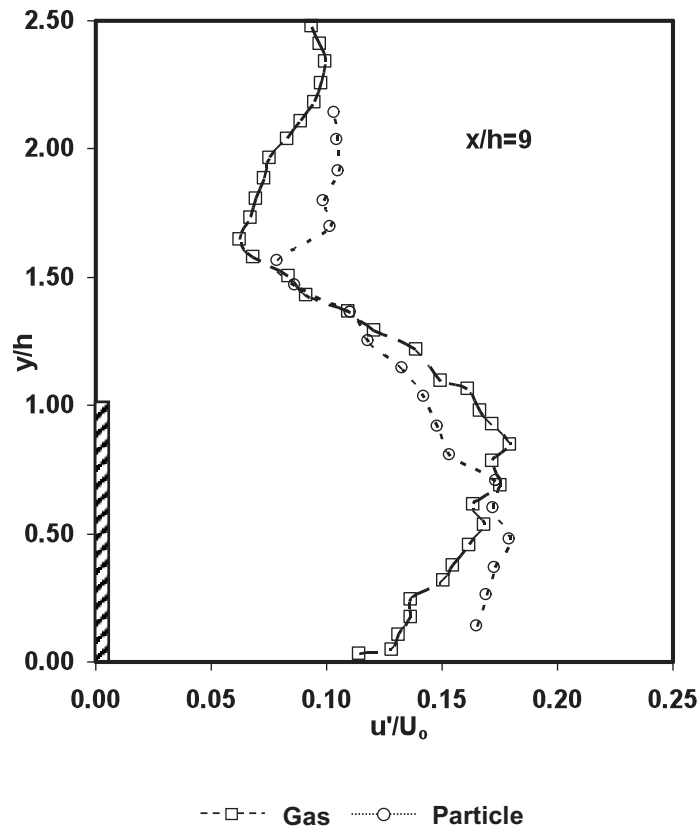Figure 5c. Experimental mean fluctuating velocities at x/h=7 for gas-particle flow

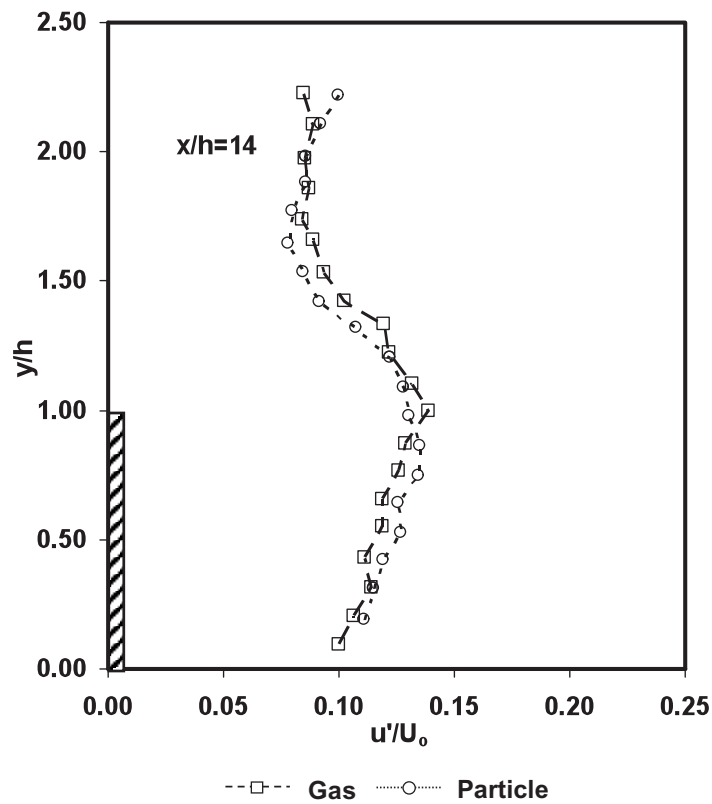Figure 5d. Experimental mean fluctuating velocities at x/h=9 for gas-particle flow



Figure 5e. Experimental mean fluctuating velocities at x/h=14 for gas-particle flow

**Numerical Code Validation:**

In this section the code is validated for mean streamwise velocities and fluctuations for both the carrier and dispersed phases against the benchmark experimental data of Fessler and Eaton (1995) for GP flow and the experimental data of Founti and Klipfel (1998) for the LP flow. This task is undertaken to verify the fact that particulate flows with two varied carrier phases can be handled by the code.

Figure 6a shows the numerical findings of single phase, diesel oil against the experimental data of Klipfel and Founti (1998) at the mean velocity level. The velocities are normalized against the freestream velocity $U_o$. Although the overall behaviour is replicated numerically there have been some under prediction for a height of y/h>1 for mid-section of the geometry, while a minor over prediction is felt along the entire height near the exit for section x/h=15.7. Figure 6b shows the fluctuating liquid velocities along the step compared against the experimental findings, there have been minor some under prediction for a height of y/h<1 at some sections, while the majority of the results show a good comparison with the experimental data. Figure 6c depicts the numerical comparison of the mean axial particulate velocities compared against the experimental data. Here again, there have been some over prediction at the last section near the exit of the geometry, while the rest of the sections agree well with the experimental data. Figure 6d depicts the experimental and numerical comparison of particle mean and fluctuating velocities and it can be seen that overall numerical results have a good agreement with the experimental data. It is also worthwhile to note that the fluctuating velocities of the particles show a better agreement using a two-fluid model rather than using a Lagrangian particle tracking approach, as they still suffer from predicting the right turbulence interactions between the two phases, which hinders from effecting a two-way coupling
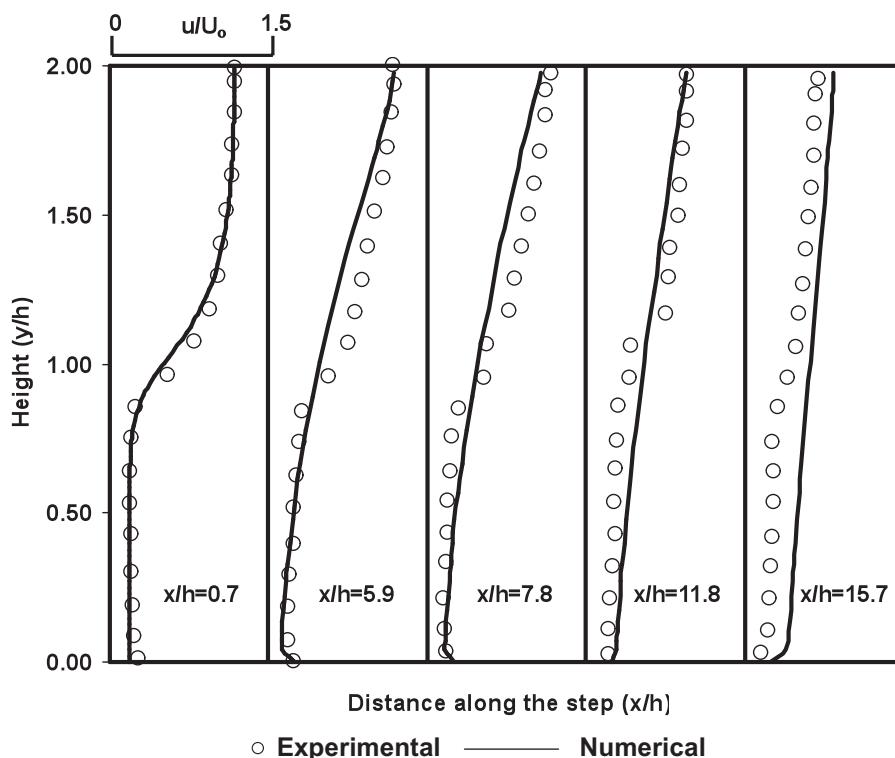


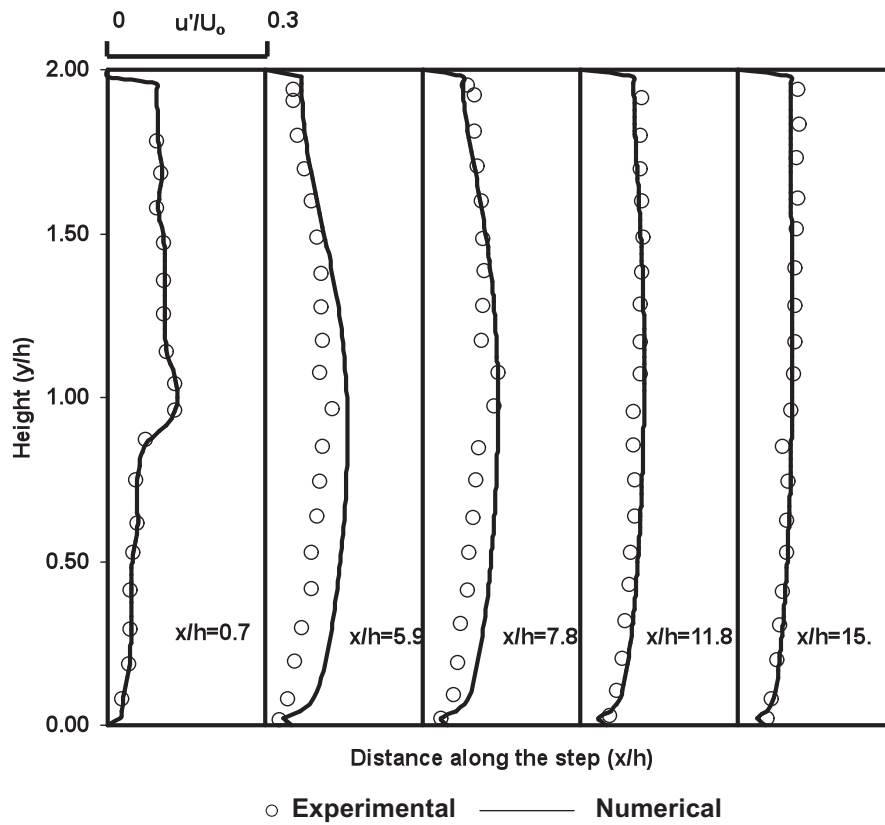Figure 6a. Axial liquid velocities along the step for LP flows

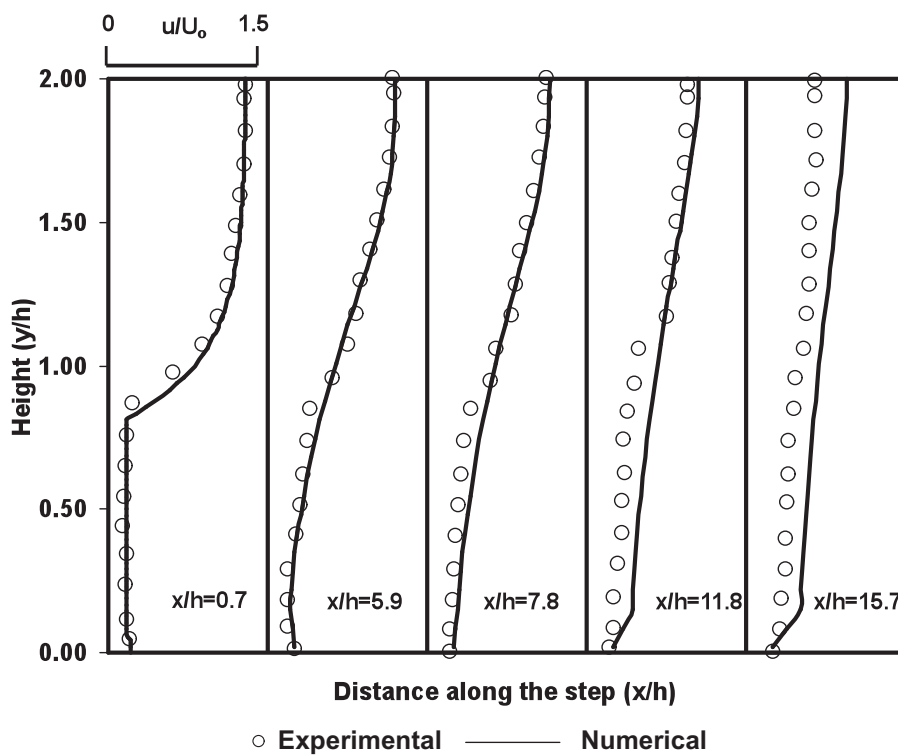Figure 6b. Fluctuating axial liquid velocities along the step for LP flows



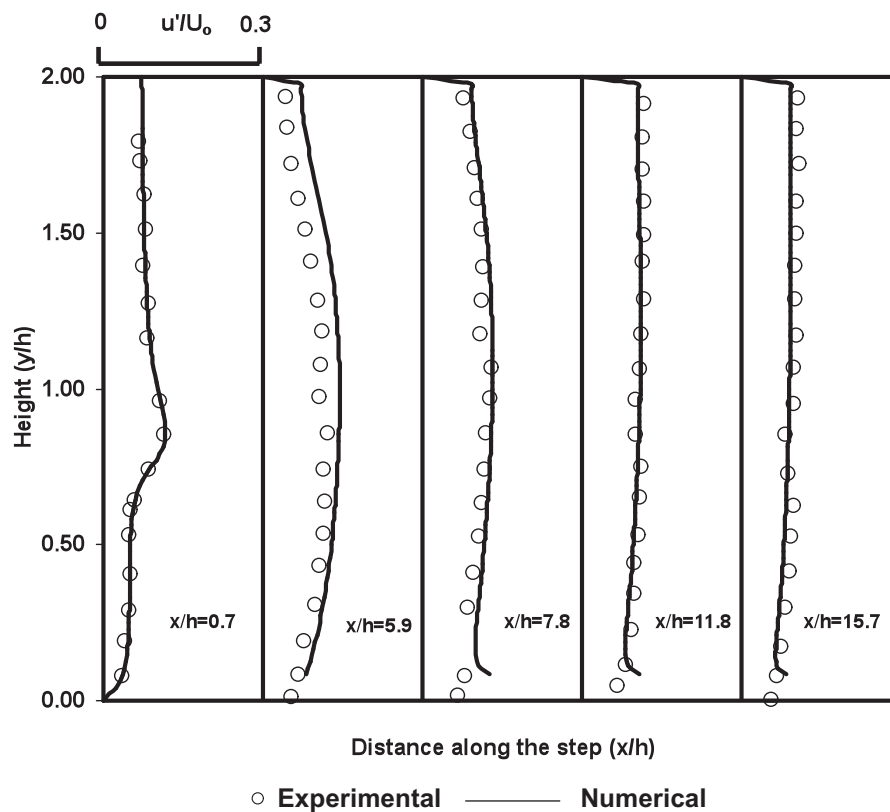Figure 6c. Axial particle velocities along the step for LP flows particles

Figure 6d. Fluctuating axial particle velocities along the step for LP flows

With the LP flow showing satisfactory agreement, the code is further validated to substantiate the numerical findings of GP flows against the experimental data of Fessler and Eaton (1995). Figure 7a shows the numerical comparison against the experimental findings and it can be seen that a fairly good agreement have been obtained between the experimental and its numerical counterpart, minor under prediction have been observed within a height of y/h<1 for the first two sections considered along the step. Figure 7b shows the mean streamwise fluctuating velocities along the step and it can be there is a general under prediction along the length of the step with some minor over prediction for a height of y/h<1 at section x/h=2. But however, the trend as seen from the numerical simulation is in lines with the experimental data. Figure 7c shows the comparison of the mean streamwise particle velocities for the 150µm glass particle against its experimental counterpart, it can be seen that there is a good agreement between the experimental and the numerical findings all along the step. The simulated streamwise fluctuating velocities for particles are compared against the experimental findings in figure 7d and it can be seen that a fairly good agreement is felt along various sections of the backward-facing step geometry.

From the comparisons of the GP flows, it is worth while to note, that mean velocities of the particles are lower at x/h=2 at the entry of the step than the gas phase, this is similar to the fully developed channel flow before the step, as reported in the experiments of Kulick et al.(1999), wherein the particles at the channel centreline exhibit lower streamwise velocities than that of the fluid as a result of cross-stream mixing. However, the gas velocity lags behind the particles aft of the step as particle inertia is slower to respond to the adverse pressure gradient than that of the fluid. At the fluctuation level, the particles exhibit higher values than the gas which again is attributed to the cross-stream mixing (Kulick et al.; 1999).
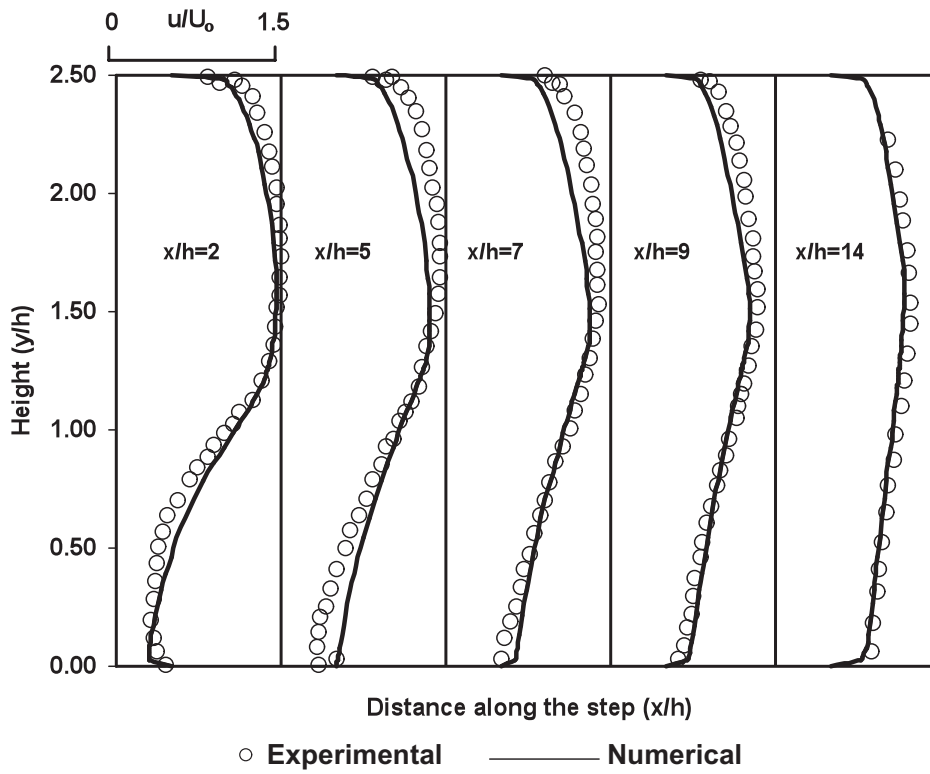
Figure 7a. Streamwise gas velocities along the step for GP flows
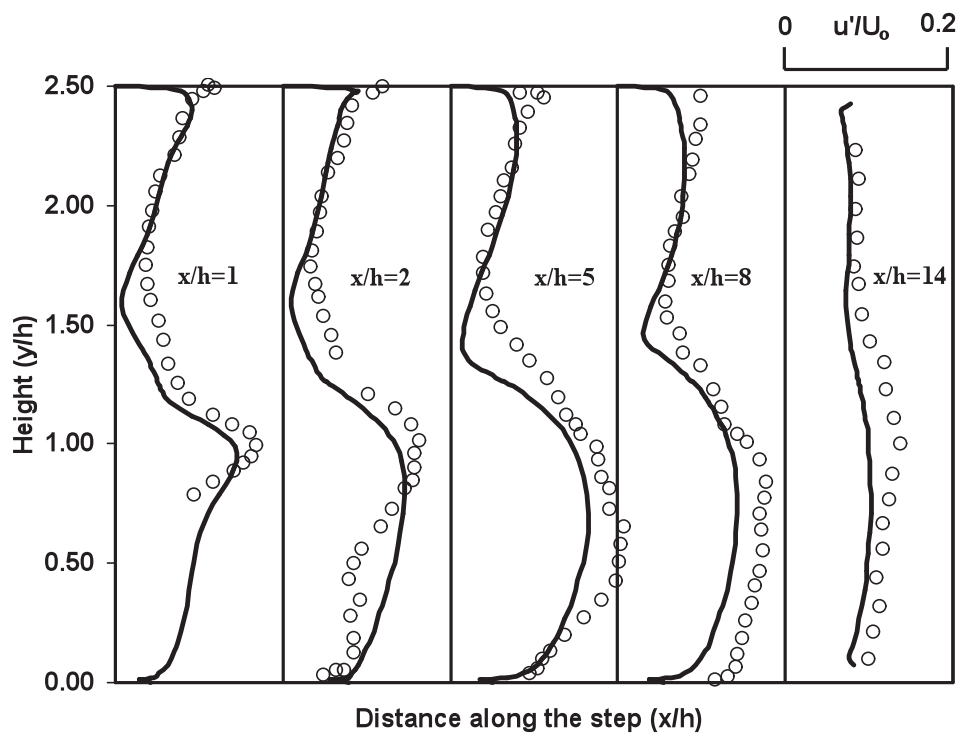


Figure 7b. Fluctuating streamwise gas velocities along the step for GP flows
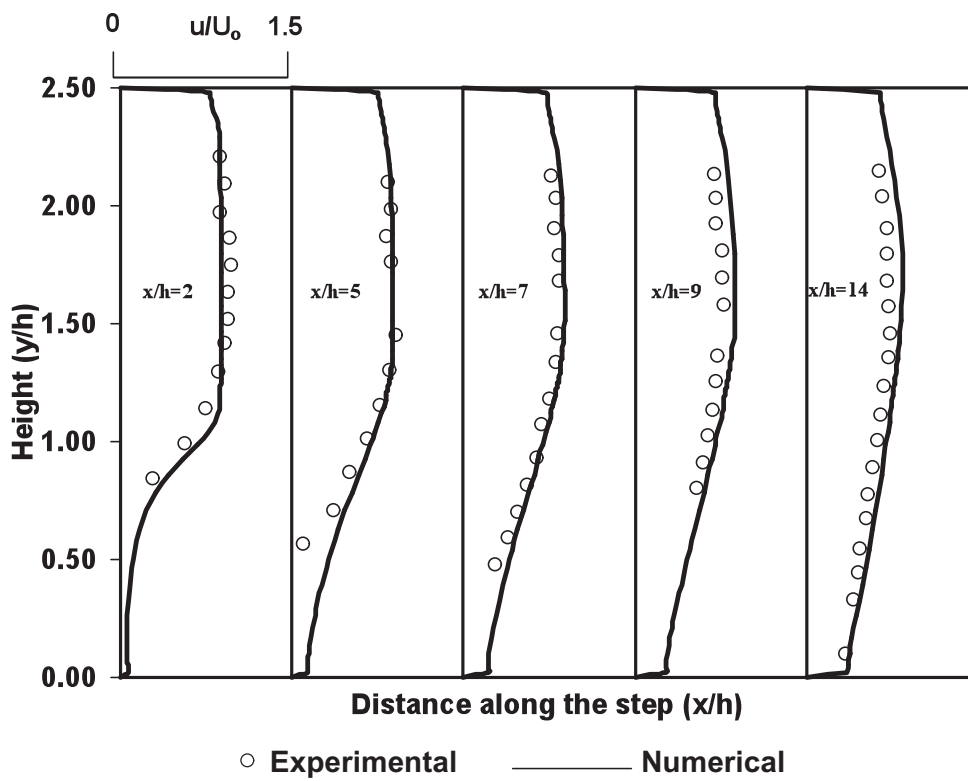
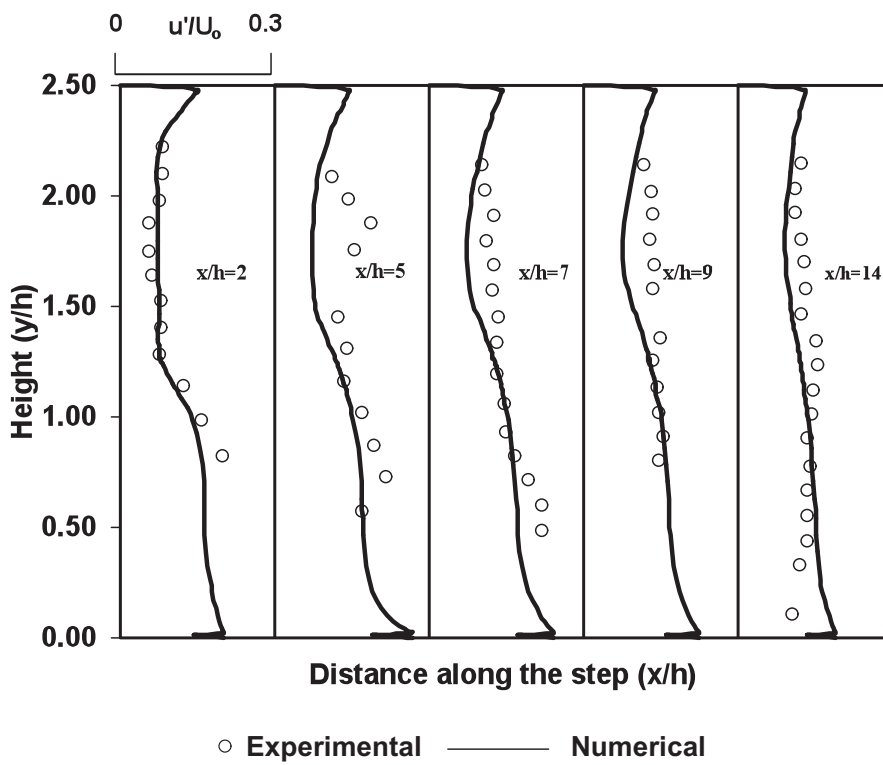Figure 7c. Streamwise mean velocity for 150 $\mu$m glass particles



Figure 7d. Fluctuating streamwise particle velocities for 150 $\mu$m glass particles

## CONCLUSION

The mean and turbulent behaviour of particles under the influence of two carrier phases namely the gas and liquid are compared and analysed, using two varying sets of experimental data behind a backward facing step geometry. From the two sets of experimental data, it can be stated that at the mean velocity level, the particles seem to 'lead' and later 'catch up' with the carrier phase for the LP flow, whereas they 'lag' behind and later 'lead' for the GP flow. At the fluctuation level, the particles seem to 'lag' and then 'catch up' for the LP flow while they 'lag' and phenomenally 'lead' for the GP flow.

Further the code was numerically validated against the benchmark experimental data of Fessler and Eaton (1995) for GP and the experimental data of Founti & Klipfel (1998) for the LP flows. Overall the numerical results revealed good agreement with the experimental data. The detailed study undertaken in this paper for turbulent particulate flows within two different carrier phases, in order to study the particle response both at the mean velocity and at the turbulence level, behind a shear flow sudden expansion geometry is quite unique and one of its kind, as there is no current published work dealing with the analysis and numerical validation of the same.

## REFERENCES

Alajbegovic A, Assad A, Bonetto F, Lahey Jr RT, Phase distribution and turbulence structure for solid/fluid upflow in a pipe. *Int. J. Multiphase flow*. 1994; 20: 453-479.

Anderson TB, Jackson R. A fluid mechanical description of fluidized beds: equations of motion. *Ind. Eng. Chem. Fundam.* 1967; 6: 527–539.

Borowsky J, Wei T. Kinematic and Dynamic Parameters of a Liquid-Solid Pipe Flow using DPIV/Accelerometry. *J. of Fluids Engg*. 2007; 129: 1415-1421.

Chan CK, Zhang HQ, Lau KS. Numerical simulation of gas-particle flows behind a backward-facing step using an improved stochastic separated flow model. *Comput. Mech*. 2001; 27: 412–417.

Chen XQ, Pereira JCF. Computational modelling of a dilute turbulent liquid-solid flow using a Eulerian-Lagrangian approach. *Int. J. of Numerical Methods for Heat & Fluid Flow*. 2001; 10: 409-431.

Clift R, Grace JR, Weber ME. Bubbles, Drops and Particles. Academic Press, New York, 1978.

Fessler JR, Eaton JK. Particle-turbulence interaction in a backward-facing step flow. *Mech. Engng Dept. Rep. MD-70*. Stanford University, Stanford, California. 1995.

Fessler JR, Eaton JK. Particle-Response in a Planar Sudden Expansion Flow. *Expt. Thermal and Fluid Science*. 1997; 15: 413-423.

Fessler JR, Eaton JK. Turbulence modification by particles in a backward- facing step flow. *J.Fluid Mech*. 1999; 394: 97-117.

Founti M. and Klipfel A. Experimental and computational investigations of nearly dense two-phase sudden expansion flows. *Experimental Thermal and Fluid science*. 1998; 17: 27-36.

Gosman AD, Ioannides E. Aspects of computer simulation of liquid-fuelled combustors. 1981. *AIAA Paper 81-0323*.

Hishida K, Maeda M. Turbulence Characteristics of Particle-Laden Flow Behind a Reward Facing Step. *ASME FED*. 1999; 121: 207-212.

Huang XY, Stock DE, Wang LP. Using the Monte-Carlo Process to simulate two-dimensional Heavy Particle Dispersion. *ASME-FED, Gas-Solid flows*. 1993; 166: 153-160.

Ishima T, Hisanobu K, Naoki S, Tomio O. Turbulence characteristics in two-phase pipe flow lading with various particles. S3_Thu_B_50, ICMF 2007, Leipzig, Germany, July 9-13, 2007.

Inthavong K, Tian ZF, Li, HF, Tu JY,Yang W, Xue CL, Li CG. A Numerical Study of Spray  Particle Deposition in a Human Nasal Cavity. *Aerosol Science and Technology*. 2006; 40: 1034-1045.

Ishii. M., Thermal-Fluid Dynamic Theory of Two-phase Flow, Eyrolles, Paris, 1975.

Kulick JD, Fessler JR, Eaton JK. Particle response and turbulence modification in fully developed channel flow. *J. Fluid Mech*. 1994; 277: 109-134.

Mohanarangam K, Tu JY. Two-fluid model for particle-turbulence interaction in a backward-facing step. *AIChE Jour*nal. 2007; 53: 2254-2264.

Pandya RVR, Mashayek F. Two-Fluid Large-eddy Simulation approach for Particle-laden Turbulent Flows. *Int. J. Heat Mass Transfer*. 2002; 45: 4753–4759.

Parthasarathy RN, Faeth GM. Structure of Particle-Laden Turbulent Water Jets in Still Water. *Int. J. Multiphase Flow*. 1987; 13: 699-716.

Parthasarathy RN, Faeth GM. Turbulence Modulation in homogenous dilute particle-laden flows. *J. Fluid Mech*. 1990; 220: 485-514.

Pawel K, Alex CH, Rudolf K. Dust lifting behind shock waves: comparison of two modelling techniques. *Chem Engg Sc*. 2005; 60: 5219-5230.

Rashidi M, Hetsroni G, Banerjee S. Particle-Turbulence Interaction in a Boundary Layer. *Int. J. Multiphase Flow*. 1990; 16: 935-949.

Righetti M, Romano GP. Particle- fluid interactions in a plane near-wall turbulent flow. *J.Fluid.Mech*. 2007; 505: 93-121.

Ruck B, Makiola B. Particle Dispersion in a Single-Sided Backward-Facing Step Flow. *Int. J. Multiphase Flow*. 1988; 14: 787-800.

Sato Y, Hishida K. Transport process of Turbulence energy in particle-laden turbulent flow. *Int. J. Heat & Fluid Flow*. 1996; 17: 202-210.

Schuh MJ, Schuler CA, Humphrey JAC  Numerical Calculation of particle-laden gas Flows Past Tubes. *AIChE J*. 1989; 35: 466-480.

Shirolkar JS, Coimbra CFM, McQuay Q. Fundamental Aspects of modeling turbulent Particle Dispersion in Dilute Flows. *Prog. Energy Combust. Sci*. 1996; 22: 363–399.

Tu JY, and Fletcher CAJ. Numerical Computation of Turbulent Gas-Solid Particle Flow in a 90º bend. *AIChE J*. 1995; 41: 2187–2197.

Tu JY. Computational of Turbulent Two-Phase Flow on Overlapped Grids.  *Numer. Heat Transfer Part B Fundam*. 1997; 32: 175–195.

Tu JY, Fletcher CAJ, Morsi YS, Yang W, Behnia M. Numerical and Experimental Studies of Turbulent Particle-Laden Gas Flow in an in-line Tube Bank, *Chem. Eng. Sci*. 1998; 52: 225– 238.

Yakhot V, Orszag SA. Renormalization group analysis of turbulence I. basic theory. *J. Sci. Comput*. 1983; 1: 3-51.

Yu KF, Lau KS, Chan CK. Large Eddy simulation of particle-laden turbulent flow over a backward-facing step. *Non-linear Sc. and Numerical Simulation*. 2004; 9: 251-262.

Zhang HQ, Yang WB, Chan CK, Lau KS. Comparison of three separated flow models. *Comput. Mech*. 2002; 28: 469–478.

## NOMENCLATURE

| | |
|---|---|
| $B_{gp}, B_{\varepsilon}$ | model constants for the Eulerian two-fluid model |
| $C_{\mu}$ | coefficient in the RNG $k$-$\varepsilon$ turbulence model |
| $C_{\varepsilon 1}, C_{\varepsilon 2}$ | model constants for standard and RNG $k$-$\varepsilon$ turbulence models |
| $d_P$ | particle diameter |
| $f$ | correction factor for drag force |
| $F_D$ | aerodynamic drag force |
| $F_G$ | gravity force |
| $F_{WMi}$ | wall-momentum transfer due to particle-wall collision force |
| $g$ | gravitational acceleration |
| $GP$ | gas particle flow |
| $I_{gp}$ | turbulence interaction between the fluid and particle phase for the particle |
| $k$ | phase turbulent fluctuating energy |
| $LP$ | liquid particle flow |
| $P_{fp}$ | turbulence production by the mean velocity gradients of two phases |
| $P_P$ | production term of the particle fluctuating energy |
| $R$ | strain rate |
| $Re$ | Reynolds number |
| $S_{\Phi}$ | source term |
| St | Stokes number |
| $S_{ij}$ | strain rate |
| $TM$ | Turbulence Modulation |
| $t_P$ | particle relaxation time |
| $t_s$ | system response time |
| $u,v,w$ | velocities in x, y &z directions respectively |
| $U_o$ | inlet bulk velocity |

*Greek letters*

| | |
|---|---|
| $a$ | **i**nverse Prandtl number |
| $\beta$ | model constant for RNG $k\text{-}\varepsilon$ turbulence model |
| $\varepsilon$ | dissipation rate of turbulent kinetic energy |
| $\eta$ | function defined in Equation (4) |
| $\eta_O$ | model constant for RNG $k\text{-}\varepsilon$ turbulence model |
| $k$ | turbulent kinetic energy |
| $v$ | kinematic viscosity |
| $\theta$ | angle between velocities of the particle and gas |
| $\rho$ | density |
| $\sigma$ | turbulence Prandtl number |
| $\Pi_{fp}$ | turbulence interaction between the fluid and particulate phases |

*Subscripts*

| | |
|---|---|
| $f$ | fluid phase |
| $fp$ | fluid-particle |
| $p$ | particle phase |
| $l$ | laminar phase |
| $T$ | turbulent flow |

*Superscript*

| | |
|---|---|
| $(\ \ )'$ | fluctuation |
| $(\overline{\ \ })$ | Favre-averaged |